

MINIATURIZATION OF INERTIAL MAGNETOELECTRIC VIBRATION VELOCITY SENSOR WITH HIGH FREQUENCY RESPONSE AT LOW FREQUENCY BAND

¹ XI CHEN, ² SHUIBAO YU

¹ College of Mathematics, Physics and Information Engineering, Zhejiang Normal University, Jinhua, 321004, Zhejiang, China.

² College of Mathematics, Physics and Information Engineering, Zhejiang Normal University, Jinhua, 321004, Zhejiang, China.

E-mail: ¹ chenxi@zjnu.cn, ² ysb101@zjnu.cn

ABSTRACT

The frequency response of the inertial magnetoelectric vibration velocity sensor is limited in the low frequency range due to the character of second order high pass filter of the structure. For better performance in the low frequency range, the traditional method is to increase the initial mass of the sensor which will increase the size and weight tremendously. This paper presents a frequency-selected compensation network to improve the performance of the frequency response at low frequency band, keeping the sensor in small size and light weight. The frequency-selected network, which is composed of amplifiers, resistors and capacitors, is connected to the output port of the sensor in cascade without any modification of the sensor's structure. After compensation, the frequency band of the sensor is flattened and the frequency response still has the character of second order high pass filter while the resonant frequency decreases from 10Hz to about 0.9Hz. The experimental results have shown that the sensor after been compensated has good performance in the low frequency range.

Keywords: *Magnetoelectric Vibration Velocity Sensor, Compensation Network, Transfer Function, Resonant Frequency, Low Frequency Band*

1. INTRODUCTION

Some vibrations, such as seismic wave, bridge vibration, vibration of water turbine, have no static reference point relative to inertial space. Low frequency components in these vibrations are always ignored since the small acceleration values could hardly be experienced. But in some area, such as industrial machines, it is significant to monitor low frequency vibrations which are vital indicators of their health [1]. Low frequency vibration detection in these fields is mainly based on high sensitivity, excellent performance, good reliability inertial sensor which has frequency range from 1Hz to 1 kHz at least [2–4]. Several kinds of sensors have been proposed in relevant researches to detect the absolute vibration (The vibration which has no static reference point relative to inertial space), such as fiber optic sensor based on Fiber Bragg Grating (FBG) [5–8], piezoelectric vibration sensor [9–11], magnetoelectric velocity sensor or accelerometer [12, 13]. In every particular

application, there has the most appropriate sensor for it [14].

One of the most widely used sensors in the low frequency absolute vibration detection is the inertial magnetoelectric velocity sensor which has the advantages of wide bandwidth (10-1000Hz), low output impedance, high resolution and low cost [15–16]. All inertial sensors using an electrical field share a basic structure called spring-mass system [17, 18]. The inertial magnetoelectric velocity sensor with this structure has the character of second order band pass filter. In this case, the measurement of low frequency is limited due to the high frequency resonance.

To improve the output signals from the inertial magnetoelectric velocity sensor in the range of low frequency, one of the methods is to increase the inertial mass to decrease the sensor's resonant frequency [19]. As a result, the size and weight of the sensor have been increased tremendously. In this situation, the mass loading can affect the

dynamic characteristics of the structure to which it is mounted [20]. The typical practice to eliminate the mass loading effect is to use the lightest, smallest sensor that still satisfies all the performance requirements [14]. So it is significant to use efficient method for frequency response improvement at the condition of keeping the light and small spring-mass system.

In this paper, we investigated the amplitude-frequency characteristic of the inertial magnetoelectric velocity sensor. According to its model and transfer function, an optimized frequency-selected compensation network was put forward which expand the working bandwidth in the low frequency range. After compensation, it still has the advantages of fast real-time response, light and small spring-mass system.

2. SENSOR MODEL

An inertial magnetoelectric velocity sensor is a mass supported on a spring and driven by an external force. The force in small sensor is normally generated electromagnetically. The suspended mass can either be the magnets with a supporting structure or in some cases the coil itself. A mechanical model of the inertial magnetoelectric velocity sensor is shown in Fig. 1.

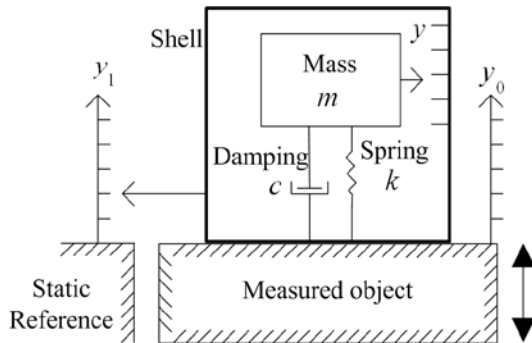


Fig. 1. Mechanical Model Of An Inertial Magnetoelectric Velocity Sensor

It can be modeled by a simple spring-mass-damping assembly where m is the inertial mass, k is spring constant and c is the damping.

Supposing y_1 is absolute coordinate of the inertial mass, y_0 is convected coordinate and y represents the relative coordinate, the motion equation can be described as

$$\frac{dy_1}{dt} = \frac{dy_0}{dt} + \frac{dy}{dt}$$

According to Newton's second law, the kinetic equation can be established as

$$m \frac{dy_1^2}{d^2t} = -c \frac{dy}{dt} - ky \quad (2)$$

And the electromagnetic induction equation can be expressed as

$$E(t) = BNL \frac{dy(t)}{dt} = \alpha \frac{dy(t)}{dt} \quad (3)$$

where B is the magnetic induction intensity, N is the number of coil turns, L is the average length of single-turn coil, $\alpha = BNL$ is the sensitivity. Assuming the exciter is making periodic sinusoidal vibration

$$y_0 = A \sin \omega t \quad (4)$$

Then the solution of equation (2) can be given by

$$y = A_1 e^{-\xi_0 \omega_0 t} \sin(\omega' t + \varphi') + A' \sin(\omega t - \varphi) \quad (5)$$

where

$$A' = A \omega'' / \sqrt{(1 - \omega''^2)^2 + (2\xi_0 \omega'')^2} \quad (6)$$

$$\tan \varphi = 2\xi_0 \omega'' / (1 - \omega''^2) \quad (7)$$

Here, A_1 , ω' , φ' is constant, $\omega'' = \omega / \omega_0$, f_0 is resonant frequency,

$$\omega_0 = 2\pi f_0 = \sqrt{k/m} \quad (8)$$

is angular frequency of the sensor,

$$\xi_0 = c / 2\sqrt{mk} \quad (9)$$

is damping ratio. The first term in equation (5) will decrease rapidly with the increase of time. Therefore, it could be approximately written as follows

$$y = A' \sin(\omega t - \varphi) \quad (10)$$

It can be concluded from equation (10) that the inertial mass is making sinusoidal vibration and the vibration frequency is the same with the measured

object. When $\omega'' \gg 1$ and $\xi_0 < 1$, i.e., the vibration frequency of the measured object is much larger than the resonant frequency of the spring-mass-damping system, it can be obtained that

$$A' = A, \quad \tan \varphi = 0. \quad \text{Hence, we have} \quad y = A' \sin(\omega t - \varphi) = A \sin(\omega t - \pi) = -A \sin(\omega t) \quad (11)$$

$$\frac{dy_0}{dt} + \frac{dy}{dt} = 0 \quad (12)$$

It means that the mass is in static state in absolute coordinate while the shell is making the same movement with the measured object.

For mechanical structure's sake, the minimum value of the resonant frequency could only be made at about 5-10Hz at best. According to equation (8),

decreasing the value of spring constant k , or increasing the inertial mass m could reduce the resonant frequency. In gravity field, the displacement y' of the spring can be expressed as

$$y' = \frac{mg}{k} = \frac{g}{(\omega_0)^2} = \frac{g}{(2\pi f_0)^2} \quad (13)$$

where g is constant of gravity acceleration.

Supposing the resonant frequency $f_0 = 1$ Hz, it could be calculated from equation (13) that the spring static elongation is more than 25cm long. Obviously, the size of the sensor is increased out of the requirement and the stability could hardly be satisfied.

3. COMPENSATION

3.1 Principle of Compensation

Applying Laplace transform to equations (1) – (3), the transfer function of the sensor can be deduced as

$$H(s) = \frac{-\alpha s^2}{s^2 + 2\xi_0\omega_0 s + \omega_0^2} \quad (14)$$

where $s = j\omega$, $\omega = 2\pi f$. Using equation (14), the magnitude and phase response of the sensor as a function of frequency and damping ratio can be calculated as shown in equation (15) and (16) respectively,

$$|H(j\omega)| = \frac{\alpha\lambda_0^2}{\sqrt{[1-(\lambda_0)^2]^2 + (2\xi_0\lambda_0)^2}} \quad (15)$$

$$\phi = \tan^{-1}\left[-\frac{2\xi_0\lambda_0}{1-\lambda_0^2}\right] \quad (16)$$

where $\lambda_0 = f / f_0$. Equation (14) shows that the transfer function has the character of second order high pass filter.

As shown in Fig. 2, it is feasible to seek a compensation network connected to the sensor in cascade when the compensated sensor system still has the character of second order high pass filter and the resonant frequency of the compensated sensor system is much lower than the uncompensated ones. The transfer function of the compensated sensor system can be expressed as

$$G(s) = \frac{V_o}{V_i} = H(s) \cdot C(s) = \frac{-\alpha s^2}{s^2 + 2\xi_0\omega_0 s + \omega_0^2} \cdot C(s) \quad (17)$$

$$= \frac{-\alpha s^2}{s^2 + 2\xi_1\omega_1 s + \omega_1^2}$$

where ω_1 is equivalent angular frequency of the sensor system after been compensated, ξ_1 is equivalent damping ratio.

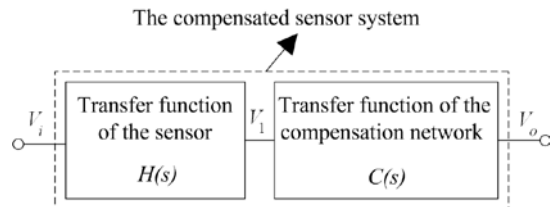


Fig. 2. Schematic Of Amplitude-Frequency Characteristic Compensation

The magnitude and phase response of the compensated sensor system as can be calculated as

$$|G(j\omega)| = \frac{\alpha\lambda_1^2}{\sqrt{[1-(\lambda_1)^2]^2 + (2\xi_1\lambda_1)^2}} \quad (18)$$

$$\phi = \tan^{-1}\left[-\frac{2\xi_1\lambda_1}{1-\lambda_1^2}\right] \quad (19)$$

where $\lambda_1 = f / f_1$, f_1 is equivalent resonant frequency. The transfer function of the compensation network, from equation (17), can be written as

$$C(s) = \frac{s^2 + 2\xi_0\omega_0 s + \omega_0^2}{s^2 + 2\xi_1\omega_1 s + \omega_1^2} = C_{HP}(s) + C_{BP}(s) + C_{LP}(s) \quad (20)$$

where

$$C_{HP}(s) = \frac{s^2}{s^2 + 2\xi_1\omega_1 s + \omega_1^2} \quad (21)$$

$$C_{BP}(s) = \frac{2\xi_0\omega_0 s}{s^2 + 2\xi_1\omega_1 s + \omega_1^2} \quad (22)$$

$$C_{LP}(s) = \frac{\omega_0^2}{s^2 + 2\xi_1\omega_1 s + \omega_1^2} \quad (23)$$

Equation (20) is a second order all-pass network which frequency response is frequency-selected. The principle block diagram is shown in Fig. 3.

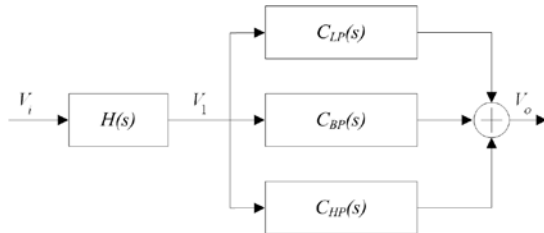


Fig. 3. Principle Block Diagram Of Frequency-Selected Compensation

3.2 Realization of Compensation

The realization of the frequency-selected compensation is shown in Fig. 4. It can be concluded that

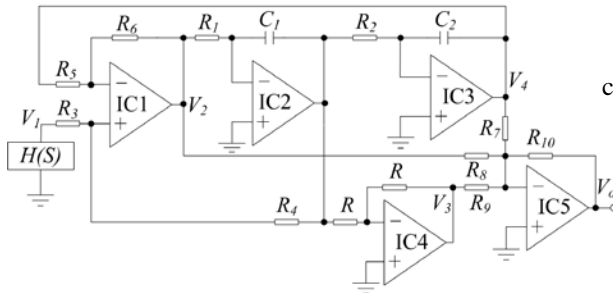


Fig. 4. Circuit Diagram Of The Frequency-Selected Compensation Network

$$\frac{V_2(s)}{V_1(s)} = \frac{\frac{R_5 + R_6}{R_5} \cdot \frac{R_4}{R_3 + R_4} s^2}{s^2 + \frac{R_5 + R_6}{R_5} \cdot \frac{R_4}{R_3 + R_4} \cdot \frac{s}{R_1 C_1} + \frac{R_6}{R_5} \cdot \frac{1}{R_1 R_2 C_1 C_2}} \quad (24)$$

$$\frac{V_3(s)}{V_1(s)} = \frac{\frac{R_5 + R_6}{R_5} \cdot \frac{R_4}{R_3 + R_4} \cdot \frac{s}{R_1 C_1}}{s^2 + \frac{R_5 + R_6}{R_5} \cdot \frac{R_4}{R_3 + R_4} \cdot \frac{s}{R_1 C_1} + \frac{R_6}{R_5} \cdot \frac{1}{R_1 R_2 C_1 C_2}} \quad (25)$$

$$\frac{V_4(s)}{V_1(s)} = \frac{\frac{R_5 + R_6}{R_5} \cdot \frac{R_4}{R_3 + R_4} \cdot \frac{1}{R_1 R_2 C_1 C_2}}{s^2 + \frac{R_5 + R_6}{R_5} \cdot \frac{R_4}{R_3 + R_4} \cdot \frac{s}{R_1 C_1} + \frac{R_6}{R_5} \cdot \frac{1}{R_1 R_2 C_1 C_2}} \quad (26)$$

Supposing $C_1 = C_2 = C$, $R_5 = R_6 = R_3 = R_4 = R$, $R_{10} = R_8$, $R_2 = 2R_1 = 2R$, then equations (24) – (26) can be simplified as

$$\frac{V_2(s)}{V_1(s)} = \frac{s^2}{s^2 + \frac{s}{RC} + \frac{1}{2R^2 C^2}} \quad (27)$$

$$\frac{V_3(s)}{V_1(s)} = \frac{\frac{s}{RC}}{s^2 + \frac{s}{RC} + \frac{1}{2R^2 C^2}} \quad (28)$$

$$\frac{V_4(s)}{V_1(s)} = \frac{\frac{1}{2R^2 C^2}}{s^2 + \frac{s}{RC} + \frac{1}{2R^2 C^2}} \quad (29)$$

$C(s)$ can be expressed as

$$C(s) = - \left[\frac{R_{10} V_2(s)}{R_8 V_1(s)} + \frac{R_{10} V_3(s)}{R_9 V_1(s)} + \frac{R_{10} V_4(s)}{R_7 V_1(s)} \right] = - \left[\frac{s^2 + \frac{R_{10} s}{R_9 RC} + \frac{R_{10}}{R_7 2R^2 C^2}}{s^2 + \frac{s}{RC} + \frac{1}{2R^2 C^2}} \right] \quad (30)$$

Comparing equation (20) with (30), it can be concluded that

$$\xi_1 = \frac{\sqrt{R_2/R_1}}{2} = \frac{\sqrt{2}}{2} \quad (31)$$

$$f_1 = \frac{1}{\sqrt{R_1 R_2 C_1 C_2}} = \frac{1}{2\sqrt{2}\pi RC} \quad (32)$$

$$\xi_0 = \frac{\sqrt{2R_7 R_{10}}}{2R_9} \quad (33)$$

$$f_0 = \sqrt{\frac{R_{10}}{2R_7}} \frac{1}{2\pi RC} \quad (34)$$

Equation (31) and (32) mean the equivalent damping ratio ξ_1 and equivalent resonant frequency f_1 of the compensated sensor system were determined by the R-C (resistance-capacitance) parameters of the circuit. The damping ratio ξ_0 and resonant frequency f_0 of the original sensor will influence the summation factor of the circuit.

3.3 Simplification of Compensation Network

For miniaturization of the sensor system, not only the sensor should be smaller, but also the compensation network need be simplified. Supposing the transfer function of the compensation network can be expressed as

$$C'(s) = \frac{s^2 + 2\xi_0 \omega_0 s + \omega_0^2}{s^2 - 2\xi_1 \omega_1 s + \omega_1^2} \quad (35)$$

Then the transfer function of the compensated sensor system can be expressed as

$$G'(s) = H(s) \cdot C'(s) = \frac{-\alpha s^2}{s^2 - 2\xi_1 \omega_1 s + \omega_1^2} \quad (36)$$

The magnitude and phase response of the compensated sensor system can be calculated as

$$|G'(j\omega)| = \frac{\alpha \lambda_1^2}{\sqrt{[1 - (\lambda_1)^2]^2 + (2\xi_1 \lambda_1)^2}} \quad (37)$$

$$\phi' = \tan^{-1} \left[\frac{2\xi_1 \lambda_1}{1 - \lambda_1^2} \right] \quad (38)$$

Comparing equation (18) with (37), (19) with (38), it could be concluded that the sensor system using these two kinds of compensation networks has the same magnitude response while the phase response is reverse.

Supposing $f_0 = 10$ Hz, $f_1 = 1$ Hz, $\xi_1 = 0.707$, $\xi_0 = 0.707$, $\alpha = 1$, the simulation curves of the normalized frequency response before and after compensation can be plotted as shown in Fig. 5. The simulation curves of phase response before and after compensation are shown in Fig. 6. Obviously, the sensor has much better performance in frequency response at low frequency band after been compensated.

From Fig. 6, it can be seen that there is a corresponding time lag associated with a sensor's output when compared to the input at frequencies near the natural frequency of the sensor. Data collected using the sensor is subject to considerable phase shifts when its frequency content is around the natural frequency of the sensor. The smaller phase errors, the more accurate data analysis will be.

The compensation network $G(s)$ translates the curve of the phase response to lower frequency direction, keeping the curve shape unchangeable. As a result, the compensated sensor has less phase error than the original one at the same frequency point. And both the phase response of the compensation network $G'(s)$ and $G(s)$ have the same phase error. Therefore, according to equation (35), the circuit of compensation network could be simplified as shown in Fig. 7.

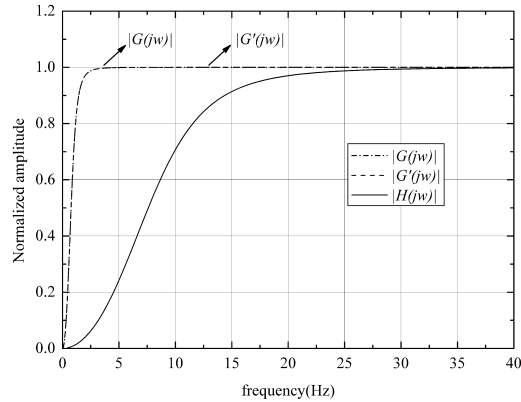


Fig. 5. Simulation Curves Of The Normalized Frequency Response Before And After Compensation ($f_0 = 10$ Hz, $f_1 = 1$ Hz, $\xi_1 = \xi_0 = 0.707$, $\alpha = 1$)

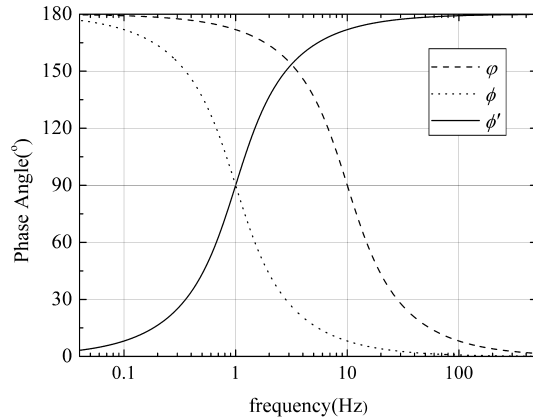


Fig. 6. Simulation Curves Of Phase Response Before And After Compensation ($f_0 = 10$ Hz, $f_1 = 1$ Hz, $\xi_1 = \xi_0 = 0.707$, $\alpha = 1$)

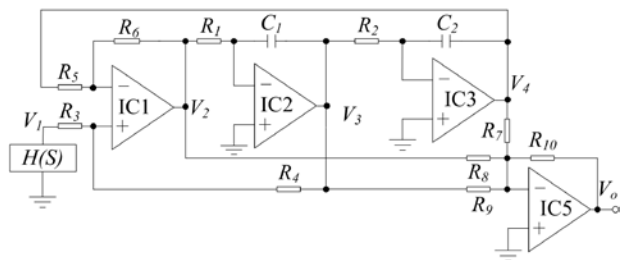


Fig. 7. Simplified Circuit Diagram Of The Frequency-Selected Compensation Network

4. EXPERIMENT AND RESULTS

4.1 Experimental Setup

The model of the original sensor we manufactured is named as CS-CD-005. The experimental setup used is shown schematically in Fig. 8. The CS-CD-005 sensor with compensation

network was rigidly mounted on the vibration table (another commercially available inertial magnetolectric velocity sensor, Bently 9200 from GE Measurement & Control Solutions, was also mounted on the vibration table for comparison test) which has the capability of controlling the vibration parameters precisely. The sensor was exposed to sinusoidal forces at different frequencies. The output signals from the sensors and compensation network were measured using a digital oscilloscope without any external signal conditioner or amplifier.

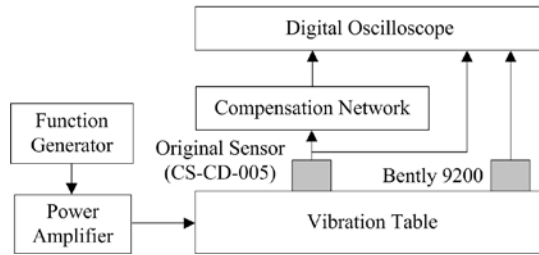


Fig. 8. Experimental system for vibration test

4.2 Parameters Determination

The nominal resonant frequency f_0 of the CS-CD-005 sensor and the damping ratio ξ_0 is undetermined. The exact value of f_0 and ξ_0 can be obtained as follows: get a group of normalized amplitudes $A_1, A_2, A_3, \dots, A_n$ with corresponding frequencies $f_1, f_2, f_3, \dots, f_n$, substituting them into equation (15), we get

$$A_n = \frac{1}{\sqrt{\left[1 - \left(\frac{f_0}{f_n}\right)^2\right]^2 + \left(2\xi_0 \frac{f_0}{f_n}\right)^2}} \quad (39)$$

where n is natural number. Therefore, f_0, ξ_0 can be derived as equation (40) and (41).

$$f_0 = \frac{f_n}{\sqrt{\left(1 - 2\xi_0^2\right) + \sqrt{\left(1 - 2\xi_0^2\right)^2 + \left(\frac{1}{A_n^2} - 1\right)}}} \quad (40)$$

$$\xi_0 = \frac{\sqrt{2f_0^2 f_n^2 - f_n^4 + f_0^4 \left(\frac{1}{A_n^2} - 1\right)}}{2f_0 f_n} \quad (41)$$

Solving equation (40) and (41) yields n solutions of f_0 and ξ_0 . The average value of f_0 and ξ_0 was used as final resonant frequency and

damping ratio.

The test results at 200mm/s velocity is shown in table 1. The calculated average value of the resonant frequency f_0 was 10.409Hz and the damping ratio ξ_0 was 0.523. Therefore, the main parameter values of the compensation network can be determined as shown in table 2. Fig. 9 is a photograph of the actual sensor that has been compensated by frequency-selected network.

Table I
Experimental Data Of Frequency Response For The Original Sensor Cs-Cd-005

Frequency f_n (Hz)	Normalized amplitude A_n
5	0.276
10	0.869
15	1.141
20	1.103
30	1.003

Table II
Main Parameter Values Of The Compensation Network

Parameters	Values	Parameters	Values
ξ_1	0.707	R (k Ω)	120
f_1 (Hz)	0.9328	R_7 (k Ω)	1.02
R_8 (k Ω)	127	R_9 (k Ω)	15.4
R_{10} (k Ω)	127	C (μ F)	1

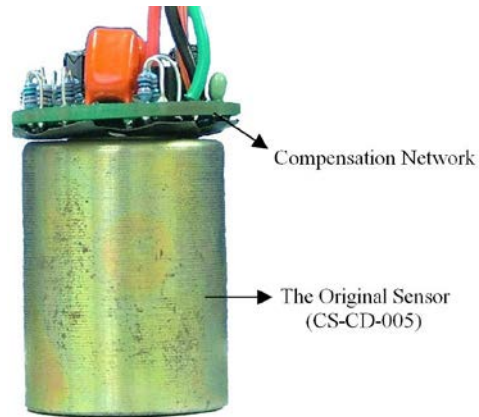


Fig. 9. Photograph Of The Sensor With Frequency-Selected Compensation Network

4.3 Experimental Setup

A clear comparison between the theoretical normalized frequency response and the

experimental ones before and after compensation is shown in Fig. 10. It shows that the experimental normalized frequency response is very close to the theoretical ones. Some experimental data deviated from the theoretical curve is due to an approximation of the R , C value. The normalized frequency response before compensation has small resonant peak and was flattened after been compensated.

Experimental comparison between 9200 and compensated CS-CD-005 were also carried out. The main parameters for comparison are listed in table 3. The sensor CS-CD-005 we used for compensation has much smaller size and weight than 9200, but higher resonant frequency. However, the resonant frequency of the CS-CD-005 sensor decreases from 10Hz to 0.93 Hz after been compensated while it still keeps the small size and light weight.

Table III
Main Parameters For Comparison Between 9200 And Compensated Cs-Cd-005

Parameters	9200	CS-CD-005	Compensated CS-CD-005
Height (mm)	102	33	43.1
Diameter (mm)	41	26	28.5
Weight(g)	480	78	90.2
Frequency Response (Hz, -3dB)	5-1000	10-1000	0.93-1000
Sensitivity (mV/(mm·s ⁻¹), 100Hz)	20	100	100
Dynamic Operating Range (mm)	2.54	2.0	2.0

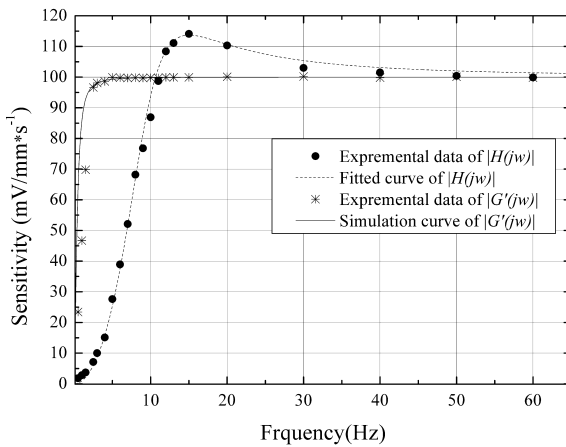


Fig. 10. Experimental And Theoretical Frequency Responses Before And After Compensation

($f_0 = 10.409$ Hz, $f_1 = 0.9328$ Hz, $\xi_0 = 0.523$, $\xi_1 = 0.707$)

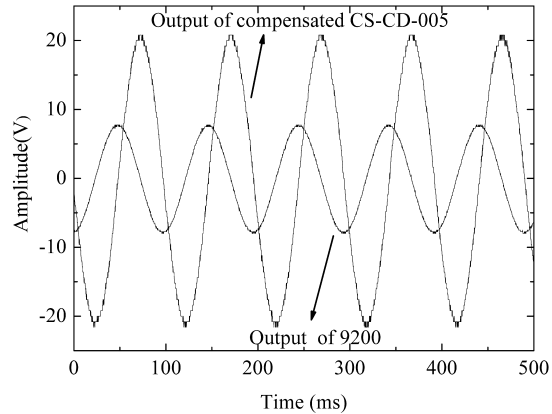


Fig. 11. Output Waveform Quality Comparison Between 9200 And Compensated CS-CD-005 At Sinusoidal Excitation Of 10 Hz, 400mm/S

The comparison of the output waveform quality between 9200 and compensated CS-CD-005 at different frequencies with the same sinusoidal excitation velocity is shown in Figs. 11-14. Obviously, the compensated CS-CD-005 has better performance in frequency response in the low frequency range. It should be pointed out that the output waveform of 9200 has little distortion at 0.4Hz while the compensated ones of CS-CD-005 still has good waveform quality. Both 9200 and compensated CS-CD-005 output waveforms were distorted seriously at 0.2Hz. However, the output waveform of compensated CS-CD-005 can still reflect the characteristic of sinusoidal vibration while the ones of 9200 is submerged in noise.

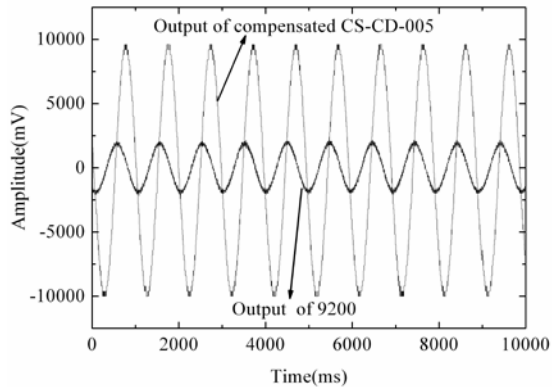


Fig. 12. Output Waveform Quality Comparison Between 9200 And Compensated CS-CD-005 At Sinusoidal Excitation Of 1 Hz, 200mm/S

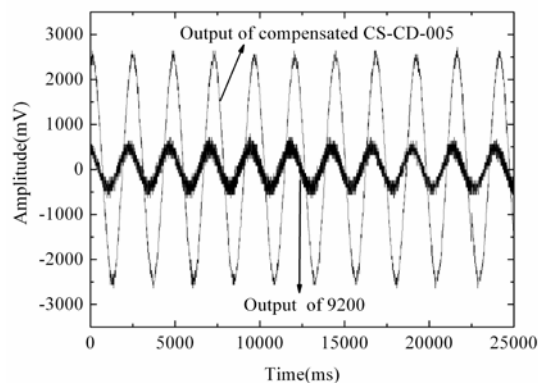


Fig. 13. Output Waveform Quality Comparison Between 9200 And Compensated CS-CD-005 At Sinusoidal Excitation Of 0.4Hz, 200mm/S

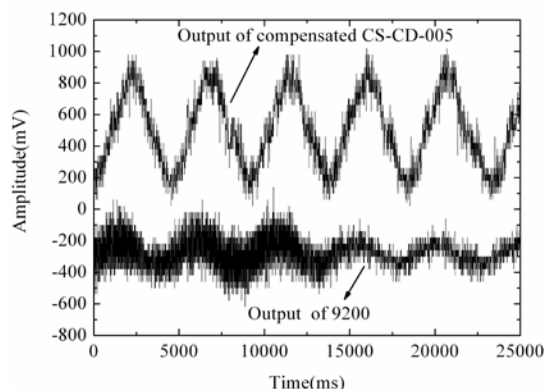


Fig. 14. Output Waveform Quality Comparison Between 9200 And Compensated CS-CD-005 At Sinusoidal Excitation Of 0.2Hz, 200mm/S.

5. CONCLUSION

The inertial magnetoelectric velocity sensor has the character of second order high pass filter and the resonant frequency cannot be very low according to the mechanical model. Since the frequency response cannot meet the demand in the low frequency range, the scope of application is limited. To improve the performance at low frequency, a frequency-selected network for amplitude-frequency characteristic compensation was developed. Experimental verification was performed and found to be in good agreement with the theoretical analysis.

At the circumstance of unchanging the original sensor's structure, the frequency-selected network improved the frequency response in the low frequency range by changing the R , C parameters of the circuit. Therefore, it still has the characters of small size and light weight. It can meet the demand in vibration measurement especially in the low frequency range.

ACKNOWLEDGEMENTS

This work was supported in part by the Science and Technology Hall of Zhejiang Province in China under Grant 2009C31006.

REFERENCES:

- [1] T. K. Gangopadhyay, Prospects for Fibre Bragg Gratings and Fabry-Perot Interferometers in fibre-optic vibration sensing, *Sensors and Actuators A*, vol. 113, n. 1, pp. 20–38, 2004.
- [2] T. C. Liang, Y. L. Lin, Ground vibrations detection with fiber optic sensor, *Optics Communications*, vol. 285, n. 9, pp. 2363–2367, 2012.
- [3] Y. Itakura, N. Fujii, T. Sawada, Basic characteristics of ground vibration sensors for the detection of debris flow, *Physics and Chemistry of the Earth, Part B*, vol. 25, n. 9, pp. 717–720, 2000.
- [4] D. Pfeffer, C. Hatzfeld, R. Werthschützky, Development of an electrodynamic velocity sensor for active mounting structures, *Procedia Engineering*, vol. 25, pp. 547–550, 2011.
- [5] J. Wu, V. Masek, M. Cada, *The possible use of fiber Bragg grating based accelerometers for seismic measurements*, Canadian Conference on Electrical and Computer Engineering (Page: 860–863 Year of Publication: 2009 ISBN: 978-1-4244-3508-1).
- [6] N. Basumallick, I. Chatterjee, P. Biswa, *et al.*, Fiber Bragg grating accelerometer with enhanced sensitivity, *Sensors and Actuators A*, vol. 173, n. 1, pp. 108–115, 2012.
- [7] L. H. Kang, D. K. Kim, J. H. Han, Estimation of dynamic structural displacements using fiber Bragg grating strain sensors, *Journal of Sound and Vibration*, vol. 305, n. 3, pp. 534–542, 2007.
- [8] F. Xie, J. Ren, Z. Chen, *et al.*, Vibration-displacement measurements with a highly stabilised optical fiber Michelson interferometer system, *Optics & Laser Technology*, vol. 42, n. 1, pp. 208–213, 2010.
- [9] T. Li, Y. H. Chen, J. Ma, Frequency dependence of piezoelectric vibration velocity, *Sensors and Actuators A*, vol. 138, n. 2, pp. 404–410, 2007.
- [10] A. Yu, P. Jiang, Z. L. Wang, Nanogenerator as self-powered vibration sensor, *Nano Energy*, vol. 1, n. 3, pp. 418–423, 2012.



- [11] S. Shanmugavel, K. Yao, T. D. Luong, *et al.*, Miniaturized acceleration sensors with in-plane polarized piezoelectric thin films produced by micromachining, *IEEE Transactions on Ultrasonics, Ferroelectrics and Frequency Control*, vol. 58, no. 11, pp. 2289-2296, 2011.
- [12] S. Wakui, A. Noda, T. Akiyama, *et al.*, Development of velocity sensor with high frequency band and its application to a vibration isolate table, *Precision Engineering*, vol.31, pp. 146-155, 2007.
- [13] A. S. Ebrahim, R. S. Huang, C. Y. Kwok, A linear electromagnetic accelerometer, *Sensors and Actuators A*, vol. 44, no. 2, pp. 103-109, 1994.
- [14] J. Shieh, J. E. Huber, N. A. Fleck, *et al.*, The selection of sensors, *Progress in Materials Science*, vol. 46, no. 3-4, pp. 461-504, 2001.
- [15] X. Yi, P. Yan, H. Zhang, *et al.*, *Vibration measurement of railway bridge with seismic low-frequency transducer based on signal reconstruction technique*, Proceedings of SPIE-The International Society for Optical Engineering (Page: 201-208 Year of Publication: 1996 ISBN: 0471970247).
- [16] L. Benassi, S. J. Elliott, Active vibration isolation using an inertial actuator with local displacement feedback control, *Journal of Sound and Vibration*, vol. 278, no. 4-5, pp. 705-724, 2004.
- [17] I. Lee, G. H. Yoon, J. Park, *et al.*, Development and analysis of the vertical capacitive accelerometer, *Sensors and Actuators A*, vol. 119, no. 1, pp. 8-18, 2005.
- [18] W. Hernández, Improving the response of an accelerometer by using optimal filtering, *Sensors and Actuators A*, vol. 88, no. 3, pp. 198-208, 2001.
- [19] F. Braghin, S. Cinquemani, F. Resta, A low frequency magnetostrictive inertial actuator for vibration control, *Sensors and Actuators A*, vol. 180, pp. 67-74, 2012
- [20] O. Cakar, K.Y. Sanliturk, Elimination of transducer mass loading effects from frequency response functions, *Mechanical Systems and Signal Processing*, vol. 19, no. 1, pp. 87-104, 2005.